SOFT ROBOTS

Bioinspired dual-morphing stretchable origami

Woongbae Kim[1,2]*, Junghwan Byun[1,2]*, Jae-Kyeong Kim[1,2], Woo-Young Choi[1,2], Kirsten Jakobsen[3], Joachim Jakobsen[3], Dae-Young Lee[2,4], Kyu-Jin Cho[1,2]†

Nature demonstrates adaptive and extreme shape morphing via unique patterns of movement. Many of them have been explained by monolithic shape-changing mechanisms, such as chemical swelling, skin stretching, origami/kirigami morphing, or geometric eversion, that were successfully mimicked in artificial analogs. However, there still remains an unexplored regime of natural morphing that cannot be reproduced in artificial systems by a "single-mode" morphing mechanism. One example is the "dual-mode" morphing of *Eurypharynx pelecanoides* (commonly known as the pelican eel), which first unfolds and then inflates its mouth to maximize the probability of engulfing the prey. Here, we introduce pelican eel–inspired dual-morphing architectures that embody quasi-sequential behaviors of origami unfolding and skin stretching in response to fluid pressure. In the proposed system, fluid paths were enclosed and guided by a set of entirely stretchable origami units that imitate the morphing principle of the pelican eel's stretchable and foldable frames. This geometric and elastomeric design of fluid networks, in which fluid pressure acts in the direction that the whole body deploys first, resulted in a quasi-sequential dual-morphing response. To verify the effectiveness of our design rule, we built an artificial creature mimicking a pelican eel and reproduced biomimetic dual-morphing behavior. By compositing the basic dual-morphing unit cells into conventional origami frames, we demonstrated architectures of soft machines that exhibit deployment-combined adaptive gripping, crawling, and large range of underwater motion. This design principle may provide guidance for designing bioinspired, adaptive, and extreme shape-morphing systems.

INTRODUCTION

Adaptive and extreme shape morphing is an elegant solution in nature for adapting to and prospering in surrounding environments (*1*–*5*). The naturally organized architectures comprising many life forms often shrink, swell, or deform along prescribed geometric morphologies to produce macroscopic unique patterns of movement, exemplified by the origami-like unfolding of swellable ice plants *Delosperma nakurense* (*1*) or the geometric eversion of the spreading tentacles of terrestrial snails (*3*). The underlying principles of such biological morphing behaviors have been, in many cases, a central design strategy of current artificial shape-morphing systems (*6*, *7*). In particular, given the complexity of natural morphing principles, efforts to simplify them into "monolithic functions," such as swelling, skin stretching, origami, kirigami, or geometric eversion, enabled successful reproduction of bioinspired morphing mechanisms in artificial systems. Pioneering examples include shape-morphing composites encoded with localized swelling anisotropy (*8*–*11*), soft robots that generated mobility and functionality using sequences of skin stretching driven by either pneumatic (*12*–*15*) or electrical (*16*–*18*) stimulation, and robotic architectures capable of kinematically guided shape morphing by origami folding (*19*–*21*) or eversion of nonstretchable layers (*22*). These results have changed the way artificial systems interact with human or sophisticated environments.

Despite the achievements of biomimicry as an engineering solution, there still remains an unexplored regime of natural morphing that cannot be reproduced in artificial system by a monolithic "single-mode" morphing mechanism. For example, recent observation of *Eurypharynx pelecanoides* (commonly known as the pelican eel) shows that the inflation of the head is characterized by two functionally different modes of morphing: first the mouth unfolds and then inflates to maximize the probability of engulfing the prey (Fig. 1A and movie S1) (*23*). This embodied "dual-mode" morphing is attributed to the coexistence of folded geometry and stretchable skin of the eel's head structure, which takes advantage of both kinematically guided shape development and adaptability induced, respectively, by unfolding and skin stretching.

Taking inspiration from the design and morphing principle of the pelican eel's frames, we present entirely soft, dual-morphing architectures that can create quasi-sequential behaviors of origami unfolding and skin stretching in response to fluid pressure. We developed and characterized the fundamental building blocks (unit cell) of entirely stretchable origami that imitated the role of the pelican eel's stretchable and foldable frames. The soft-bodied architectures, whose embedded fluid paths were defined by the kinematic arrangement of such unit cells, experienced the fluid pressure distribution acting in the direction of deploying the body first and inducing skin stretching, resulting in adaptive and extreme dual-mode shape morphing. The bioinspired dual-morphing capability of our design rule was verified by reproducing the eccentric dual morphing of a live pelican eel. Using the dual-morphing stretchable origami in combination with traditional origami bases, such as Miura origami and Yoshimura origami, we achieved unexplored realms of kinematic features, locomotion and gripping mechanisms, and biomimicry.

RESULTS

Pelican eel–inspired dual-morphing stretchable origami

The pelican eel *E. pelecanoides* is a type of eel with a distinctively shaped mouth that inhabits the deep ocean. We recently spotted and filmed a bizarre-looking pelican eel that morphed in a manner not previously discovered (see Materials and Methods and note S1 for details) (*23*). The eel dramatically transformed the shape of its head

[1]Soft Robotics Research Center, Seoul National University, Seoul, Republic of Korea. [2]Department of Mechanical and Aerospace Engineering, Institute of Advanced Machines and Design, Seoul National University, Seoul, Republic of Korea. [3]The Rebikoff-Niggeler Foundation (FRN), Horta, Azores, Portugal. [4]School of Engineering and Applied Sciences and Wyss Institute for Biologically Inspired Engineering, Harvard University, Cambridge, MA, USA.
*These authors contributed equally to this work.
†Corresponding author. Email: kjcho@snu.ac.kr

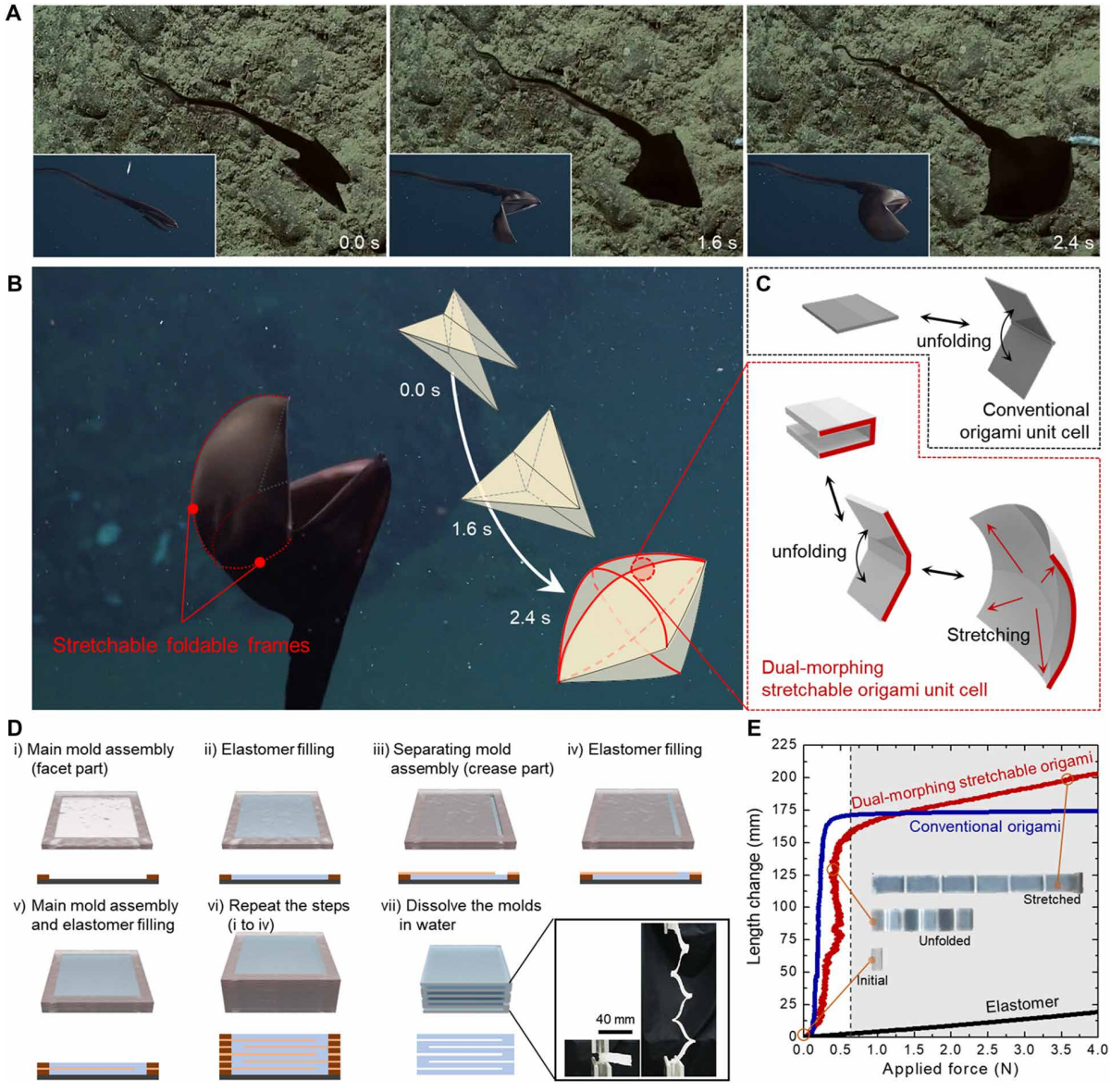

Fig. 1. Pelican eel–inspired dual-morphing stretchable origami. (**A**) The live pelican eel *E. pelecanoides* dynamically extends its mouth via dual-mode morphing (movie S1). (**B**) Morphing principle of the pelican eel interpreted by the stretchable forms of origami fish base. Red lines indicate the pelican eel's stretchable and foldable frames. (**C**) Concept of bioinspired dual-morphing stretchable origami in comparison with conventional origami. (**D**) Fabrication of dual-morphing stretchable origami. Repetitive steps of mold assembly and elastomer filling were conducted to build the architecture of C-channel origami units. A subsequent demolding process was carried out by dissolving the molds in water. The final origami architecture was not only deployable but also stretchable. (**E**) Morphing behaviors of bioinspired dual-morphing stretchable origami (red), conventional paper origami (blue), and an elastomer unit (black) in response to longitudinal stress in the direction that the system deploys. The inset images indicate the initial, unfolded, and stretched states of the dual-morphing stretchable origami.

from a folded to an inflated state suitable for hunting (Fig. 1A and movie S1). This peculiar pattern of movement is characterized by two functionally different modes of morphing that first trigger body shape development by geometric unfolding and then create additional motion by stretching the constructed body. We found that the unfolding principle of the head follows that of the fundamental origami fish base and, at the same time, it can stretch extremely due to the highly stretchable skin frame (Fig. 1B).

Inspired by the design and morphing mechanism of the pelican eel's stretchable and foldable frames, we developed synthetic origami units that can be both unfolded and stretched, achieving dual-mode morphing (Fig. 1C). A unit cell of the stretchable origami has a C-channel–shaped unit geometry that can not only share geometric similarities with conventional origami unit cells (thus able to composite nearly all types of origami architectures) but also be stretched easily (note S2). The facets and the crease line of the C-channel unit are made of the same stretchable elastomers so that deployment relies dominantly on the extreme bending of the facets near the clamped edge (Fig. 1C), whereas, in conventional origami unit cells, the difference in bending stiffness between the crease line and the facets induces unfolding (*19*–*21*, *24*, *25*). This C-channel–shaped stretchable origami unit cells can be arranged in a manner that forms

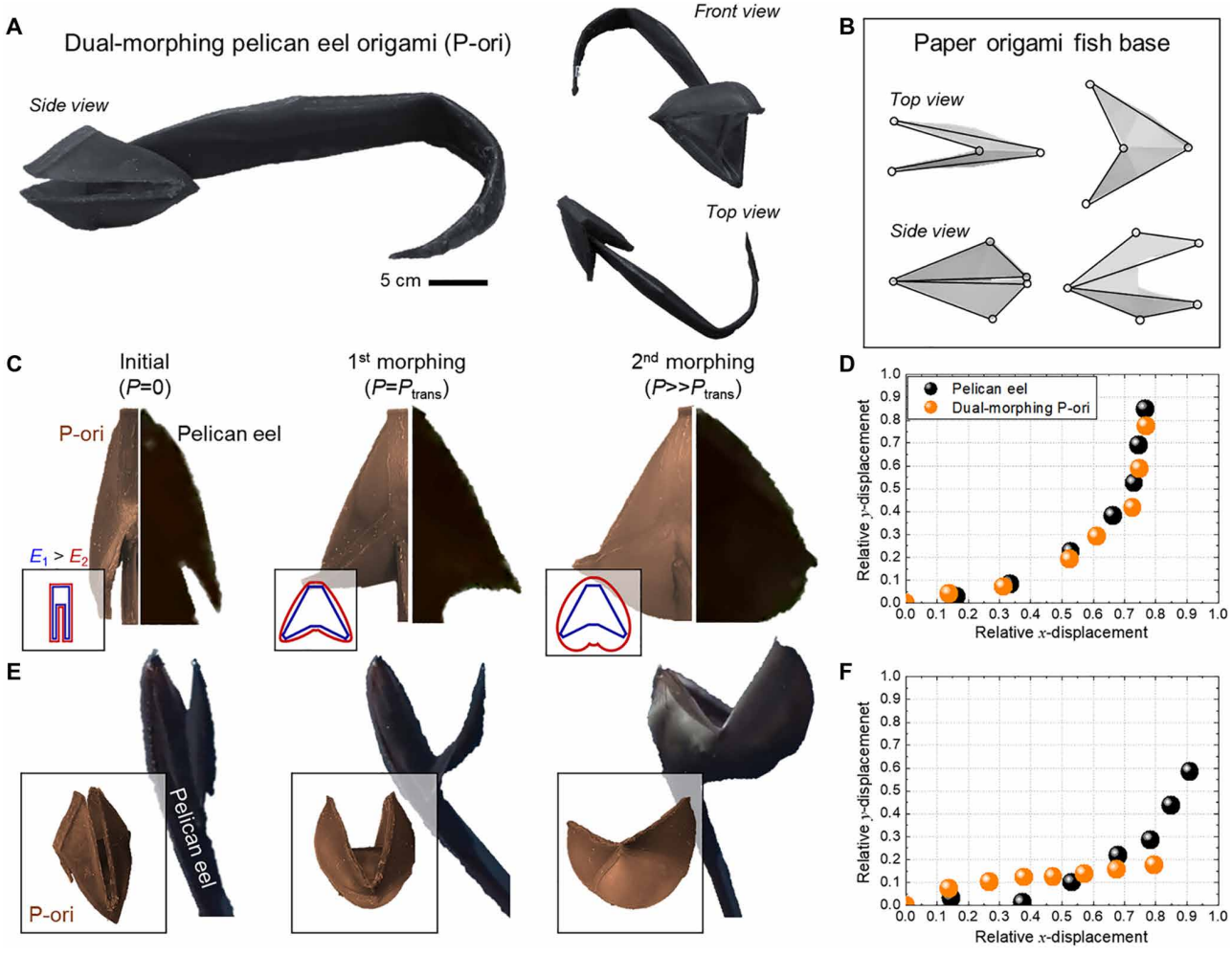

Fig. 2. A dual-morphing origami architecture mimicking a pelican eel (dual-morphing P-ori). (**A**) Dual-morphing P-ori built on double-layered origami fish base. (**B**) Geometric morphing of paper origami fish base. (**C** and **E**) Top and side views of the dual-morphing behavior of P-ori (left) and a live pelican eel (right) (movie S2). (**D** and **F**) Trajectory of the jaw end point of P-ori and a pelican eel from the top and side views (see fig. S5 for details).

fluidic channels and chambers and therefore can use the effect of material stretching for morphing as if a pneumatic network unit is being stretched due to fluid pressure (*12*–*15*). To efficiently fabricate three-dimensional (3D) architectures of unit cells, we developed a proper elastomer casting method, termed a "layer stacking method" (Fig. 1D, figs. S1 and S2, and Materials and Methods). In this method, dozens of flat, water-soluble layer molds (main, separating, and cover molds) were stacked together in alternating sequence with pouring of elastomer; after curing, the resulting structure could be obtained by dissolving the molds in water. The fabricated prototype of the six-module dual-morphing stretchable origami has a compact initial configuration and illustrates dual-morphing response with both unfolding and stretching (inset image of Fig. 1D).

The quantitative investigation of this behavior suggested that the dual-morphing behavior (red line) can be characterized by the superimposition of the geometry-driven origami unfolding (blue line) and the stretching of the elastomer (black line). We found that the geometry-driven unfolding could be completed much earlier than the stretching of the elastomer within far lower material stresses (Fig. 1D). This also indicates that robotic architectures consisting of such stretchable origami linkages can experience high levels of rapid and large-magnitude morphing without losing soft and adaptable properties through the quasi-sequential dominance shift between unfolding and stretching. Given that the unit cell of the dual-morphing stretchable origami can be considered as a stretchable plate subject to uniform pressure, the unique dual-morphing behavior is generally free from scaling issues when all geometric parameters are equally scaled while neglecting the effect of gravity. However, if the geometric values are constant but only vary in thickness (t), then bending becomes preferable to stretching as the thickness decreases because bending energy density is proportional to t^3, whereas stretching energy density is ~t. A simple pseudo-rigid body model approach also supported the scaling relationship in our dual-morphing origami design (see fig. S3 and note S3 for details on the scaling relationship).

Bio-mimicking dual-morphing pelican eel origami

To verify the effectiveness of this unconventional but "natural" origami, we built an artificial creature that mimicked the morphing of a pelican eel. The pelican eel's head can be divided symmetrically up and down against its long mouth, in which each part contains a short snout connected to the long jaws on both sides. The head is found to be an initially folded structure that spreads sideways geometrically when

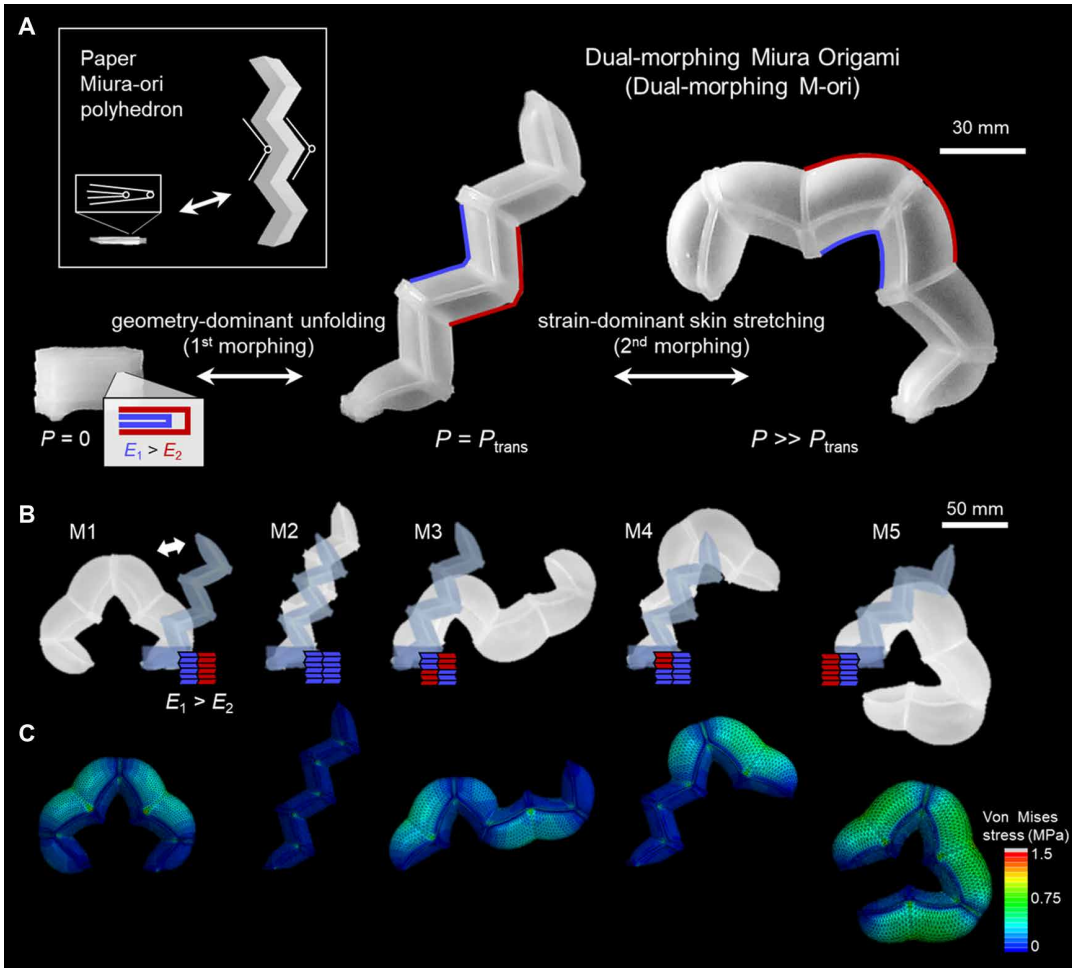

Fig. 3. Dual-morphing M-ori (dual-morphing M-ori). (**A**) Kinematic composition and dual-morphing behavior of six-module M-ori. Inset image: conventional morphing of a paper Miura-ori polyhedron (movie S3). (**B**) Programmable dual-morphing responses of M-ori with distinct material disposition. Two different elastomers [DragonSkin30 (E_1 ~ 600 kPa, highlighted in blue) and DragonSkin10 (E_2 ~ 150 kPa, highlighted in red)] were patterned into each side of the module to generate inner bending (M1), bloating (M2), S-shape (M3), and outer bending (M4 and M5) while being pressurized with air (ΔP = 15 kPa). (**C**) Investigation of morphing by FEA (see Materials and Methods).

the mouth is opened and finally inflates like a balloon. Because this unique pattern of movement is similar to the development of origami fish base, we built a pelican eel–like soft origami architecture, termed dual-morphing "P-ori," using a double-layered origami fish base structure with embedded fluid paths (the inner layer for the frame and the outer one for the skin) (Fig. 2, A and B; fig. S4, A and B; and movie S2). The dual-morphing P-ori was designed to have length ratios in the mouth and jaw parts that correspond to those of the live animal to enhance the similarity between the dual-morphing profiles. The material for the outer skin was selected to be much softer than that of the inner frame to extend the overlapping regimes of the first (geometry-dominant) and second (strain-dominant) morphing modes (note S4). This allowed notable body stretching during geometric unfolding as in the case of a live pelican eel (Fig. 2, C and E). The kinematics of the live animal and its artificial analog was analyzed to verify the successful reproduction of the dual-morphing principle by tracking the relative displacement of the jaw end point from the top and side view, with angles that were taken as close as possible to those for the live eel (Fig. 2, D and F, and fig. S5). The results suggest that our design rule that patterns dual-morphing, entirely stretchable unit cells into the origami base observed in natural life forms adequately imitated nature's solution to adaptive and extreme shape morphing, although the jaw profile from the side view exhibited a slight discrepancy due to the existence of the closing motion.

Dual-morphing Miura origami

The basic origami unit cell originated from the pelican eel's frames can extend the morphing dimension and the corresponding kinematic feature of traditional origami (*26*, *27*). We demonstrated architectures of stretchable origami that achieved extensible kinematic domains in a manner that was previously inaccessible. One typical design is dual-morphing Miura origami (M-ori), which was built on a parent Miura-ori polyhedron (*26*) (Fig. 3A; fig. S4, C and D; and note S4). By compositing dual-morphing origami unit cells in an alternatively stacked manner, we defined the embedded fluidic networks of dual-morphing M-ori. Because of the geometric correspondence with the Miura-ori polyhedron, the dual-morphing M-ori can initially exhibit origami-like morphing that enables rapid, large-magnitude, and kinematically defined deployment without structural interference between adjacent facets when unfolded (note S5). Additional pressurization causes the morphing mode to be shifted from a geometry-dominant mode to a strain-dominant mode, allowing the robot's body to stretch as a whole and create versatile "hidden soft robotic" secondary morphing [bending in an inner (M1) or outer (M4 and M5) direction, S-shape (M3), and bloating (M2)] along the engineered distribution of the material stiffness (Fig. 3, B and C, and movie S3). Attractive features of this design methodology are that the dual-morphing profile can be designed to (i) have the large-magnitude deployment at a relatively low-pressure level in comparison with the

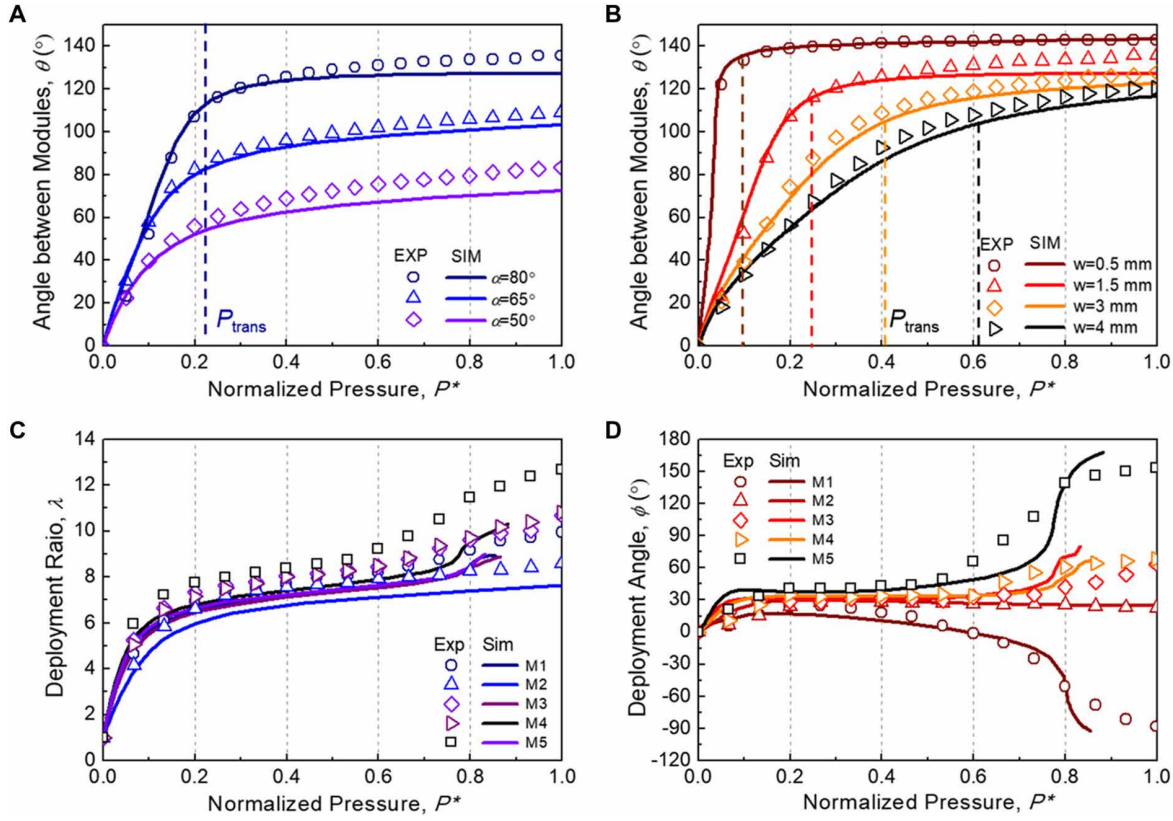

Fig. 4. Parametric study of dual-morphing M-ori. (**A** and **B**) Quantitative analysis of dual-morphing behavior of two-module M-ori for different values of geometric parameters, α (A) and *w* (B). (**C** and **D**) Experimental and simulation results of deployment ratio (λ) and deployment angle (ϕ) about five different dual-morphing M-ori shown in Fig. 3 (B and C). *P** is defined as *P*/20 (kPa/kPa) for (A) and (B) and *P*/15 (kPa/kPa) for (C) and (D).

conventional fluidic bending actuator that uses the close proximity of inflation between neighboring chambers (fig. S6) and (ii) generate the secondary stretching motion that guides the morphing in a direction different (even normal) to unfolding.

A quantitative study of the dual-morphing behavior was performed for the angle between adjacent modules (θ) and the transition pressure between the two morphing modes (P_{trans}) (Fig. 4, A and B). The experimental and finite element analysis (FEA) simulation results showed that both the dominance between each mode and the unfolding behavior could be determined by the geometric parameters (α and *w* for M-ori, defined in fig. S1D) of the parent origami frame (fig. S7). The maximum θ significantly increases from 90° to 140° as α increases from 50° to 80° (Fig. 4A and fig. S8), whereas the increase in *w* from 0.5 to 4 mm changes P_{trans} from 2 to 9 kPa (Fig. 4B). The approximate time responses of θ at each pressure level are shown in fig. S9. On the other hand, skin stretching occurs across the entire regime of applied pressure (fig. S7, E to G), which implies that the superimposition of bending and stretching results in the quasi-sequential dominance shift between the two morphing modes (also described in Fig. 1E).

The complex response of the second morphing mode was also investigated for θ, deployment ratio (λ), and deployment angle (ϕ) (figs. S10 and S11 and note S6). First, we studied the effect of the distributed stiffness on the morphing behavior of an M-ori unit module based on two elastomer mixtures with a modulus (*E*) difference [(i) $E_1 > E_2$ and (ii) $E_1 < E_2$] (fig. S10A). It is observed that the stiffness distribution causes asymmetric bending (inner or outer) of the unit module in the strain-dominant morphing mode, whereas a single-material module [(iii) $E_1 = E_2$] experiences uniform bloating (fig. S10, B to D). Extended to the multi-module dual-morphing M-ori architectures (M1 to M5, depicted in Fig. 3B), the coupled dual-morphing responses generated similar deployment vectors (λ ~ 7, ϕ ~ 30°) during the first geometry-dominant morphing mode ($0 < P \leq 3$ kPa) and featured extreme versatile secondary morphing configurations (λ > 10, −90° < ϕ < 180°), which cannot be derived from the deployment behavior of traditional M-ori (Fig. 4, C and D). In particular, we confirmed that the dual-morphing M-ori could produce a blocked tip force of ~2.8 N at ϕ = 0° through the second strain-dominant morphing that moves in a direction different to unfolding, allowing it to function as a soft actuator (fig. S12).

Soft robotic applications of dual-morphing M-ori

The dual-morphing M-ori showcases a previously unexplored class of morphing behavior in soft robotic applications. To exemplify the potential functionalities such as initial compactness and deployment-combined adaptive morphing, we demonstrated unconventional gripping and locomotion mechanisms and a soft machine that can cover a wide field of vision underwater (Fig. 5). First, we constructed a deployable soft gripping system using three six-module dual-morphing M-ori in which the second morphing mode was regulated for inner bending. The ability to change their length extremely from an initially compact design allowed the system to be portable (fig. S13 and movie

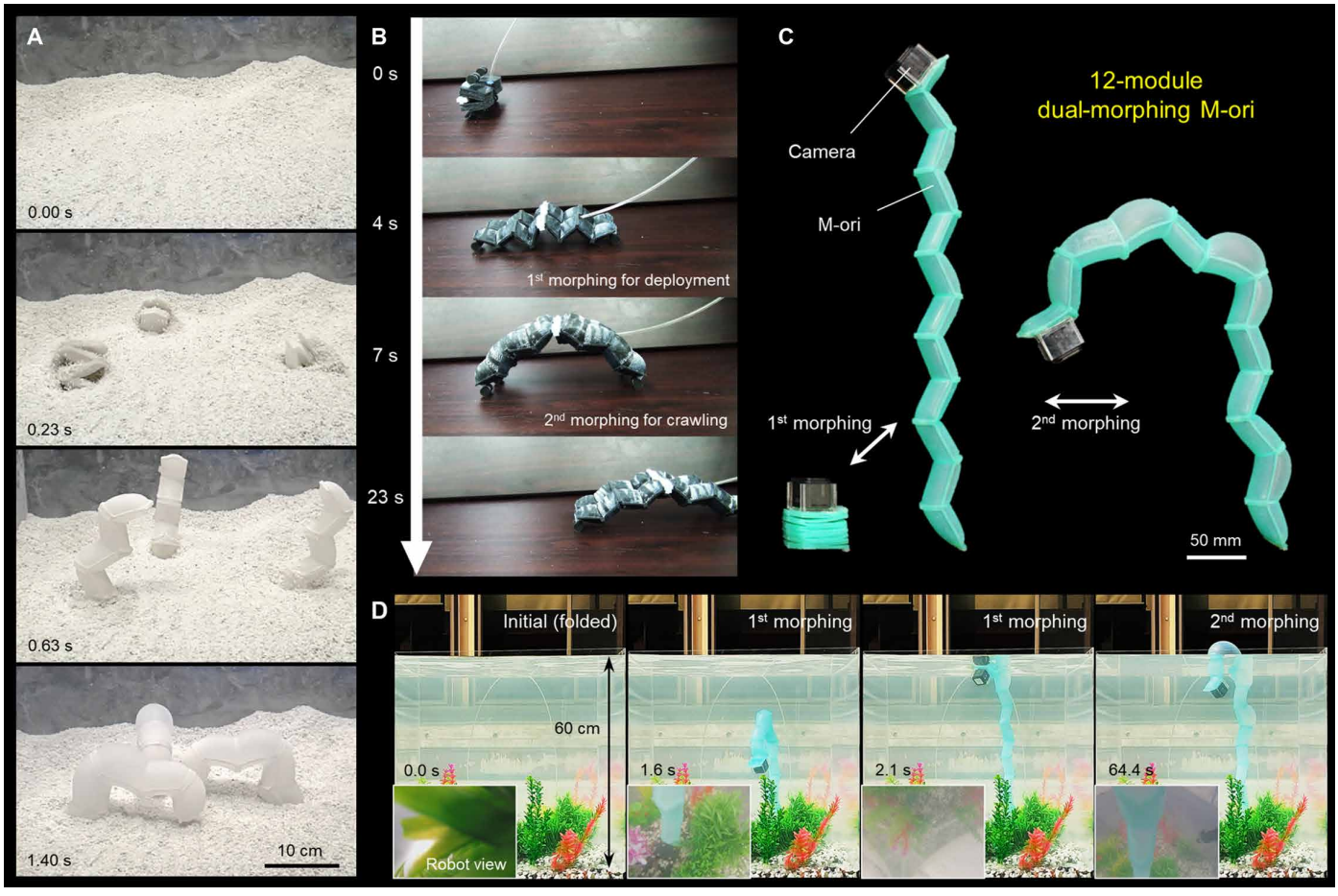

Fig. 5. Soft robots consisting of dual-morphing M-ori. (**A**) The unique behavior of dual-morphing M-ori features initial compactness (thus capable of being concealed in a heap of sand), rapid deployment (<0.4 s), and adaptive, functional morphing (movie S5). (**B**) A soft crawling robot consisting of four four-module dual-morphing M-ori demonstrates deployment-combined crawling locomotion characterized by the repeated transition in the second morphing mode (movie S6). (**C**) Soft robotic eye tentacle consisting of 12-module dual-morphing M-ori and a wireless camera. (**D**) The robot's extreme shape-changing capabilities can cover a wide field of vision (movie S7).

S4) or easily concealed inside their surrounding environment, such as in a heap of sand (Fig. 5A). It could protrude from the sand through origami-like morphing (<0.4 s) and subsequently actuate toward $\phi = -90°$ to softly but robustly grasp a fast-moving object (Kamigami Robot bug, Dash Robotics Inc.) (<1.3 s) (movie S5).

Another cooperative dual-morphing strategy enabled a robotic crawler to embody deployment-combined locomotion (Fig. 5B). We demonstrated the soft crawling robot consisting of four four-module dual-morphing M-ori to verify the enhanced mobility (or even portability) of soft robots based on our approach. The deployable soft crawler could first develop its shape to be ready for locomotion and crawled via repeated transitions in the second morphing mode of soft robotic bending motion (movie S6).

Further extreme shape morphing was showcased by a robotic eye tentacle consisting of a 12-module dual-morphing M-ori (Fig. 5C). Inspired by the eye tentacle of terrestrial snails that make a better field of vision using a dual-morphing mechanism (*3*), the robot was designed to enable extreme lengthening (more than 15 times its initial height of 36 mm) and bizarre-looking quivering by programmed material disposition (fig. S14 for the architecture of material stiffness distribution in the soft robotic eye tentacle). In addition, a wireless camera (GoPro HERO5 Session) was equipped to provide vision. Accordingly, the images captured by the robotic tentacle were collected from the deep bottom to the outside of the water. Subsequently, the embodied dual-morphing capability enabled the robot to cover a wide field of vision underwater via repeated secondary morphing (Fig. 5D and movie S7).

Dual-morphing Yoshimura origami

Similar to the dual-morphing M-ori, the stretchable origami unit cells were composited on the basis of the parent Yoshimura-ori cylinder (note S4) (*27*). The resulting dual-morphing origami architecture, termed "dual-morphing Y-ori," has strengths in symmetric growing and programmable bloating (Fig. 6A and fig. S1, E and F). The dual-morphing Y-ori was fabricated by arranging a set of dual-morphing origami unit cells mirror symmetrically. Similar to other dual-morphing origami architectures, the quasi-sequential morphing is a key mechanism that shifted dominance from geometry-dominant shape development in the height direction ($\lambda \approx 4.5$ for four-module architecture) to strain-dominant asymmetric bloating ($\lambda \approx 5.5$) (fig. S15 and movie S8). The feature that grows symmetrically in the height direction could be integrated into other dual-morphing behaviors, leading

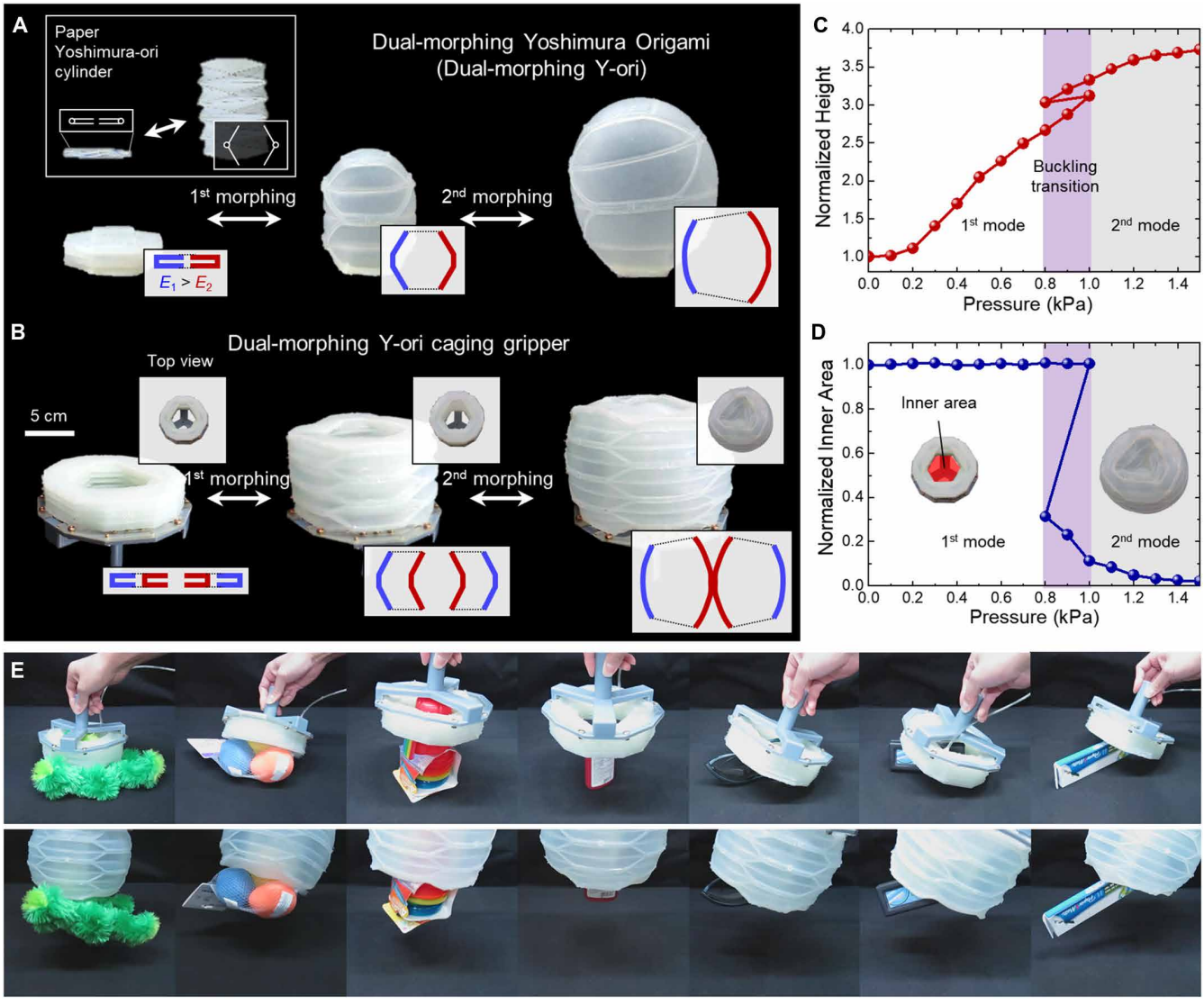

Fig. 6. Dual-morphing Y-ori. (**A**) Dual-morphing response of four-module Y-ori under fluidic pressurization compared with that of a paper Yoshimura-ori cylinder (movie S8). The insets in the bottom right corners represent schematics of the arrangement of dual-morphing origami unit cells with different stiffnesses for asymmetric bloating. (**B**) Morphing behavior and mechanism of the dual-morphing Y-ori caging gripper. The gripper consists of two eight-module dual-morphing Y-ori with a design in which the softer Y-ori is enclosed by a relatively stiffer Y-ori. The first morphing mode is characterized by linear actuation, and the second one is characterized by asymmetric bloating for adaptive gripping (movie S10). (**C** and **D**) Characterization of dual morphing of the Y-ori caging gripper. While the gripper grows in the height direction with increasing applied pressure, the inner area reduces only during the second morphing mode. (**E**) Universal dual-morphing gripping of irregular-shaped objects (movie S10).

to a class of soft robots capable of versatile, adaptive, and human-interactive tasks (fig. S16 and movie S9).

To further demonstrate the benefits of the dual-morphing Y-ori, we developed a deployable soft caging gripper that exploited dual morphing for universal grasping in a previously inaccessible manner (Fig. 6B and movie S10). The gripper was made from two dual-morphing Y-ori with different radii and material stiffnesses. In particular, the stiffness of the inner cylinder was designed to be lower than that of the outer one for asymmetric bloating. The two quasi-sequential morphing modes are functionally separated in terms of grasping ability: the first mode triggered only a body-length change ($\lambda \approx 3.1$), and the second mode performed the task of grasping by reducing the inner area of the gripper to enclose the object (Fig. 6, C and D). Compared with the existing mechanisms of universal soft grippers that used granular jamming (*28*), finger grasping (*13*), and suction (*29*), the dual-morphing mechanism allowed the gripper to grow toward the object, enclose it, and hold it. This unique gripping behavior has the advantages of protecting the object from external impact and enabling a 5-kg object to be held stably (movie S10). It also demonstrated universal gripping irrespective of the shape of objects (Fig. 6E and movie S10).

DISCUSSION

Stretchable origami frames found in nature intrinsically embody two functionally different morphing mechanisms, unfolding and stretching. We have shown that the entirely stretchable origami unit cell is the fundamental building block of the dual-morphing mechanism that

is nature's solution to adaptive and extreme shape morphing. We demonstrated some prototypes of kinematic arrangements of the unit cells for pneumatically driven dual-morphing architectures. Although made entirely of stretchable elastomers, these robotic architectures could experience rapid, large-magnitude, and kinematically defined deployment at low material stresses during the first morphing mode, suggesting a new paradigm in architecting adaptive and extreme shape-morphing system. The possibility of sharing a wide range of origami design pools, including well-known Miura and Yoshimura origami and origami bases existing in nature, enabled us to readily illustrate the versatility of artificial dual-morphing systems. We expect that our design principle is potentially applicable to other existing origami frames, such as Kresling origami or an origami magic ball that exhibits inherent twisting motion and a radial motion, respectively. Our approach offers a new platform for the material architecture and shape-morphing system that can potentially be used to realize bio-inspired morphing mechanisms, portable soft robots, biomedical devices, and active metamaterials.

MATERIALS AND METHODS

Video capturing of a live pelican eel

A live pelican eel that used dynamic dual morphing for hunting was spotted and filmed by means of the manned submersible LULA1000, operated by the Rebikoff-Niggeler Foundation in Portugal (movie S1). The observation was made in the Azores archipelago in 1000 m of depth.

Materials for bioinspired dual-morphing stretchable origami architectures

The dual-morphing origami was made of silicone rubbers or rubber-like 3D-printed materials. Commercially available highly soft and stretchable rubbers Dragonskin 10 and 30 (shore hardness A10 and A30, elongation at break of 1000 and 364%, respectively; Smooth-On Inc.) and Ecoflex 0010 (shore hardness 0010 and 800% of elongation at break; Smooth-On Inc.) were used for casting. The silicones are originally translucent white, but we used Silc Pig (Smooth-On Inc.) to color them if necessary. The 12-module dual-morphing M-ori was colored green, and the dual-morphing P-ori was colored black. For multi-material 3D printing, a rigid material (VeroWhitePlus; shore hardness 85D; Stratasys Ltd.) and a rubber-like material (TangoBlackPlus; shore harness A27 and elongation at break of 218%; Stratasys Ltd.) were used. The shore hardness of each part of the dual-morphing origami could be controlled from 27A to 95A by selectively changing the composition ratio between the two materials. For the demonstration of the 3D-printed dual-morphing M-ori used for a soft crawler, we selected TangoBlackPlus for the part of the stretchable facets and FLX9840-DM (shore hardness A35-40) for the part of the relatively stiff facets. All dual-morphing origami architectures were connected to an 1.8-mm-diameter polyurethane tube (MPUT1.8-10-C, MISUMI) for fluidic actuation.

Fabrication of dual-morphing stretchable origami architectures

A new fabrication technique called a layer-stacking method was developed that could build a soft robot architecture with complex embedded fluid channels. In this method, dozens of flat layer molds (thickness = 0.5 or 1 mm) were sequentially stacked together with the pouring of elastomer. We classified the layer molds into three types: a "main layer mold (M-mold)," a "separating layer mold (S-mold)," and a "cover mold (C-mold)" (fig. S1). The M-mold defines the shape of the main facets (and associated crease lines) of dual-morphing origami, which form origami tessellation. The S-mold, which is stacked between the two M-molds, defines the crease lines that not only separate the facet portion but also connect the crease portion. The C-mold defines the floor and cover of the completely stacked mold. All molds have holes at the sides for alignment.

The molds were made by 3D printing a water-soluble material PVA+(eSUN) or laser cutting (VLS 3.5; Universal Laser System) thin acrylic plates or paraffin wax plates with the thickness of 0.5 mm (S-mold) and 1 mm (M-mold and C-mold). After the layer molds were fabricated and coated with a silicone release agent (Ease Release 200, Mann Release Technologies Inc.), the following molding processes were carried out: First, the C-mold was placed at the bottom with pins for alignment, and the M-mold was stacked on it (Fig. 1D, i, and fig. S2A). A liquid-phase elastomer was poured into the M-mold (Fig. 1D, ii, and fig. S2B), and then the S-mold was carefully covered over the M-mold and filled with an elastomer (Fig. 1D, iii and iv, and fig. S2, C and D). In the same manner, the sequential process of stacking the M-mold, pouring a liquid-phase elastomer, and covering with the S-mold was repeated (Fig. 1D, v and vi, and figs. S2E and S3). When the layers were completely stacked, the C-mold was placed on the top to finish the process (fig. S2F). The stacked layer molds were placed in an oven for 1 hour at 65°C. After the elastomer was fully cured, the bridges were cut and the inner and outer parts of the layer mold were disconnected. Subsequently, the soluble molds (made of PVA+) were dissolved in 70°C water with a magnetic stirring process for 8 hours (Fig. 1D, vii, and fig. S2G). When insoluble molds (acrylic plates) were used, the molds were physically removed, while the material and the structure often underwent large mechanical stress and undesired deformation. Last, the remaining structure was sealed using a half-cured elastomer or a silicone adhesive (Sil-Poxy, Smooth-On Inc.) (fig. S2H). Because the width of voids of the S-molds was narrow within a few millimeters, the elastomer placed underneath the mold did not mix with that placed at the upper side of the mold. Therefore, different elastomers could be patterned individually for each M-mold, which means that stiffness could be spatially distributed for each layer (Fig. 3C). Excluding mold fabrication time, the whole process could be completed within 12 hours, and most of the process did not require any manual labor. The entire fabrication process is described in movie S11.

We also used an Objet260 Connex multi-material printer (Stratasys Ltd.) to directly fabricate the dual-morphing origami architectures. Because the multi-material 3D printer could combine two different materials to meet the desired shore A hardness ranging from 27 to 95, we could build the soft facets with different stiffnesses to design programmable motions. This direct method enabled us to fabricate nonflat foldable origami structures, such as the Kresling pattern and the origami magic ball, in which the folded geometry of the facets is not parallel to the base surface (thus difficult to fabricate by the layer stacking method). Although 3D printing enabled direct printing of complex and multi-material origami structures, it has several drawbacks, such as limited material availability, high price, and difficulty in mass production. Further, the elongation ratio of TangoBlackPlus was much lower than that of highly stretchable elastomers used in a layer stacking method (elongation limit, ~1000%), resulting in poor repeatability and robustness.

Experimental protocols for actuation

The actuation of dual-morphing origami architectures was carried out by a tethered pneumatic source. A compressor or a fluidic pump was used as an air source, and fluids were applied into dual-morphing origami through urethane tubes with the diameter of 1.8 mm. The applied pressure was regulated precisely by a pressure regulator and solenoid valves. The level of pressurization subjected to dual-morphing origami was measured by a pressure sensor.

Image analysis

Image analysis was performed to extract data from the experiments. We attached red markers at dual-morphing origami (fig. S7A). The center positions of the attached markers were found by MATLAB function "imfindcircle" and by the codes that filtered the mistaken circles by RGB data (fig. S7B). The relative coordinates of the markers were used to calculate the angle between adjacent modules (θ) (Fig. 4, A and B), deployment ratio (λ), and deployment angle (ϕ) (fig. S11). The length change of the facet was obtained by analyzing the color difference from the background; we manually selected two points and then MATLAB calculated the length of the arc between the points (fig. S7, E to G). The inner area of the dual-morphing Y-ori caging gripper was also calculated by converting the captured images into binary ones (0, black and 1, white) and finding the number of "0" pixels.

Finite element analysis

The nonlinear FEA was performed using the commercial FEA software ABAQUS (Dassault Systèmes). Material properties used in FEA (Dragonskin 30, Dragonskin 10, and Ecoflex 0010) were obtained completely from uniaxial tension tests and volumetric tests. In the software, materials were considered as a Yeoh hyperelastic material model that was matched well with the experimental results. To make the same condition with the actual experiments for the dual-morphing M-ori, we set the diamond-shaped fluidic channel of the bottom surface to a fixed boundary condition. For every case, the applied pressure was set to increase linearly and a contact condition was a "general contact." Positions of the desired nodes were collected to evaluate the angle between modules (θ), deployment ratio (λ), and deployment angle (ϕ) (fig. S11).

SUPPLEMENTARY MATERIALS

robotics.sciencemag.org/cgi/content/full/4/36/eaay3493/DC1

Note S1. Dual morphing in nature
Note S2. Design comparison between dual-morphing stretchable origami and conventional origami
Note S3. Scaling relationship of dual-morphing stretchable origami
Note S4. Parent origami frames and structural modification
Note S5. Analytic evaluation of the deployment behavior of a Miura-ori polyhedron
Note S6. Definition of the module, deployment ratio (λ), and angle (ϕ) of the dual-morphing M-ori
Fig. S1. Layer molds and a stacking order for three different dual-morphing origami architectures.
Fig. S2. Fabrication process of dual-morphing origami architectures: A layer stacking method.
Fig. S3. Scaling relationship of dual-morphing stretchable origami.
Fig. S4. Parent origami frames and arrangement of dual-morphing stretchable origami unit cells.
Fig. S5. Kinematics of pelican eel and dual-morphing P-ori.
Fig. S6. Comparison between conventional fluidic bending actuators and M-ori.
Fig. S7. Parametric study of dual-morphing M-ori.
Fig. S8. Geometry-dominant, origami-like morphing of dual-morphing M-ori with different α values.
Fig. S9. Dynamic behavior of the two-module M-ori.
Fig. S10. Strain-dominant soft robotic morphing of dual-morphing M-ori with programmed material disposition.
Fig. S11. Deployment ratio (λ) and angle (ϕ) of dual-morphing M-ori.
Fig. S12. Tip force of the six-module inner bending M-ori.
Fig. S13. A dual-morphing M-ori gripper.
Fig. S14. Architecture of material stiffness distribution in the soft robotic eye tentacle.
Fig. S15. Dual-morphing Y-ori with programmability.
Fig. S16. A dual-morphing human-interactive soft robot.
Movie S1. Dual-morphing behavior of a pelican eel.
Movie S2. Pelican eel–like morphing of a stretchable origami fish base.
Movie S3. Dual-morphing stretchable M-ori.
Movie S4. Deployable soft gripper.
Movie S5. Dual-morphing stretchable M-ori in the ground.
Movie S6. Deployable soft crawler.
Movie S7. Underwater soft tentacle.
Movie S8. Dual-morphing stretchable Y-ori.
Movie S9. Dual-morphing human-interactive soft robot for hugging.
Movie S10. Dual-morphing stretchable Y-ori soft caging gripper.
Movie S11. Layer mold stacking method.

REFERENCES AND NOTES

1. M. J. Harrington, K. Razghandi, F. Ditsch, L. Guiducci, M. Rueggeberg, J. W. C. Dunlop, P. Fratzl, C. Neinhuis, I. Burgert, Origami-like unfolding of hydro-actuated ice plant seed capsules. *Nat. Commun.* **2**, 337 (2011).
2. S. Armon, E. Efrati, R. Kupferman, E. Sharon, Geometry and mechanics in the opening of chiral seed pods. *Science* **333**, 1726–1730 (2011).
3. M. Lemaire, R. Chase, Twitching and quivering of the tentacles during snail olfactory orientation. *J. Comp. Physiol. A* **182**, 81–87 (1997).
4. K. Saito, S. Nomura, S. Yamamoto, R. Niyama, Y. Okabe, Investigation of hindwing folding in ladybird beetles by artificial elytron transplantation and microcomputed tomography. *Proc. Natl. Acad. Sci. U.S.A.* **114**, 5624–5628 (2017).
5. Y. Forterre, J. M. Skotheim, J. Dumais, L. Mahadevan, How the Venus flytrap snaps. *Nature* **433**, 421–425 (2005).
6. K. Oliver, A. Seddon, R. S. Trask, Morphing in nature and beyond: A review of natural and synthetic shape-changing materials and mechanisms. *J. Mater. Sci.* **51**, 10664–10689 (2016).
7. E. Reyssat, L. Mahadevan, Hygromorphs: From pine cones to biomimetic bilayers. *J. R. Soc. Interface* **6**, 951–957 (2009).
8. R. M. Erb, J. S. Sander, R. Grisch, A. R. Studart, Self-shaping composites with programmable bioinspired microstructures. *Nat. Commun.* **4**, 1712 (2013).
9. J. Kim, J. A. Hanna, M. Byun, C. D. Santangelo, R. C. Hayward, Designing responsive buckled surfaces by halftone gel lithography. *Science* **335**, 1201–1205 (2012).
10. A. S. Gladman, E. A. Matsumoto, R. G. Nuzzo, L. Mahadevan, J. A. Lewis, Biomimetic 4D printing. *Nat. Mater.* **15**, 413–418 (2016).
11. L. Huang, R. Jiang, J. Wu, J. Song, H. Bai, B. Li, Q. Zhao, T. Xie, Ultrafast digital printing toward 4D shape changing materials. *Adv. Mater.* **29**, 1605390 (2017).
12. R. F. Shepherd, F. Ilievski, W. Choi, S. A. Morin, A. A. Stokes, A. D. Mazzeo, X. Chen, M. Wang, G. M. Whitesides, Multigait soft robot. *Proc. Natl. Acad. Sci. U.S.A.* **108**, 20400–20403 (2011).
13. F. Ilievski, A. D. Mazzeo, R. F. Shepherd, X. Chen, G. M. Whitesides, Soft robotics for chemists. *Angew. Chem. Int. Ed.* **50**, 1890–1895 (2011).
14. B. Mosadegh, P. Polygerinos, C. Keplinger, S. Wennstedt, R. F. Shepherd, U. Gupta, J. Shim, K. Bertoldi, C. J. Walsh, G. M. Whitesides, Pneumatic networks for soft robotics that actuate rapidly. *Adv. Funct. Mater.* **24**, 2163–2170 (2014).
15. E. Siéfert, E. Reyssat, J. Bico, B. Roman, Bio-inspired pneumatic shape-morphing elastomers. *Nat. Mater.* **18**, 24–28 (2019).
16. T. Li, G. Li, Y. Liang, T. Cheng, J. Dai, X. Yang, B. Liu, Z. Zeng, Z. Huang, Y. Luo, T. Xie, W. Yang, Fast-moving soft electronic fish. *Sci. Adv.* **3**, e1602045 (2017).
17. J. Byun, Y. Lee, J. Yoon, B. Lee, E. Oh, S. Chung, T. Lee, K.-J. Cho, J. Kim, Y. Hong, Electronic skins for soft, compact, reversible assembly of wirelessly activated fully soft robots. *Sci. Robot.* **3**, eaas9020 (2018).
18. E. Acome, S. K. Mitchell, T. G. Morrissey, M. B. Emmett, C. Benjamin, M. King, M. Radakovitz, C. Keplinger, Hydraulically amplified self-healing electrostatic actuators with muscle-like performance. *Science* **359**, 61–65 (2018).
19. S.-J. Kim, D.-Y. Lee, G.-P. Jung, K.-J. Cho, An origami-inspired, self-locking robotic arm that can be folded flat. *Sci. Robot.* **3**, eaar2915 (2018).
20. S. Li, D. M. Vogt, D. Rus, R. J. Wood, Fluid-driven origami-inspired artificial muscles. *Proc. Natl. Acad. Sci. U.S.A.* **114**, 13132–13137 (2017).
21. R. V. Martinez, C. R. Fish, X. Chen, G. M. Whitesides, Elastomeric origami: Programmable paper-elastomer composites as pneumatic actuators. *Adv. Funct. Mater.* **22**, 1376–1384 (2012).
22. E. W. Hawkes, L. H. Blumenschein, J. D. Greer, A. M. Okamura, A soft robot that navigates its environment through growth. *Sci. Robot.* **2**, eaan3028 (2017).

23. F. Schembri, First direct observation of hunting pelican eel reveals a bizarre fish with an inflatable head; https://www.sciencemag.org/news/2018/10/first-direct-observation-hunting-pelican-eel-reveals-bizarre-fish-inflatable-head.
24. J. A. Faber, A. F. Arrieta, A. R. Studart, Bioinspired spring origami. *Science* **359**, 1386–1391 (2018).
25. S. Mintchev, J. Shintake, D. Floreano, Bioinspired dual-stiffness origami. *Sci. Robot.* **3**, eaau0275 (2018).
26. T. Tachi, K. Miura, Rigid-foldable cylinders and cells. *J. Int. Shell Spat. Struct.* **53**, 217–226 (2012).
27. Y. Yoshimura, "On the mechanism of buckling of a circular cylindrical shell under axial compression," report NACA-TM-1390 (National Advisory Committee for Aeronautics, 1955).
28. E. Brown, N. Rodenberg, J. Amend, A. Mozeika, E. Steltz, M. R. Zakin, H. Lipson, H. M. Jaeger, Universal robotic gripper based on the jamming of granular material. *Proc. Natl. Acad. Sci. U.S.A.* **107**, 18809–18814 (2010).
29. M. Follador, F. Tramacere, B. Mazzolai, Dielectric elastomer actuators for octopus inspired suction cups. *Bioinspir. Biomim.* **9**, 046002 (2014).

Acknowledgments: We thank M. K. Kim for her help designing the dual-morphing, human-interactive soft robot. **Funding:** This work was supported by the National Research Foundation of Korea (NRF) (NRF-2016R1A5A1938472), the Technology Innovation Program (10051287, Development of fundamental technology of soft robotics for advanced soft gripper) funded by the Ministry of Trade, Industry and Energy (MOTIE, Korea), and the KIST Institutional Program (project no. 2V07080-19-P073). **Author contributions:** W.K. designed and built the robots, performed and analyzed the experiments and simulation, and wrote the manuscript. J.B. designed and guided the experiments, analyzed the experiments and simulation, and organized and wrote the manuscript. J.-K.K. assisted in experimental works and development of the fabrication method. W.-Y.C. contributed to material testing, data analysis, and simulation. K.J. and J.J. took the first video images on a hunting pelican eel and assisted in writing of the manuscript. D.-Y.L. assisted in designing robots and writing of the manuscript. K.-J.C. directed the project and edited the manuscript. **Competing interests:** W.K., J.-K.K., and K.-J.C. are included on a Korea patent application (KR 10-2018-0081668) that covers the layer mold stacking method and stretchable origami structures, which has been submitted by SNU R&DB Foundation. The other authors declare that they have no competing interests. **Data and materials availability:** All data needed to evaluate the conclusions in the paper are present in the paper and/or the Supplementary Materials. Additional data related to this paper may be requested from the authors.

Submitted 11 June 2019
Accepted 9 October 2019
Published 27 November 2019
10.1126/scirobotics.aay3493

Citation: W. Kim, J. Byun, J.-K. Kim, W.-Y. Choi, K. Jakobsen, J. Jakobsen, D.-Y. Lee, K.-J. Cho, Bioinspired dual-morphing stretchable origami. *Sci. Robot.* **4**, eaay3493 (2019).

Science Robotics

Bioinspired dual-morphing stretchable origami

Woongbae Kim, Junghwan Byun, Jae-Kyeong Kim, Woo-Young Choi, Kirsten Jakobsen, Joachim Jakobsen, Dae-Young Lee and Kyu-Jin Cho

Sci. Robotics **4**, eaay3493.
DOI: 10.1126/scirobotics.aay3493

Science Robotics (ISSN 2470-9476) is published by the American Association for the Advancement of Science, 1200 New York Avenue NW, Washington, DC 20005. The title *Science Robotics* is a registered trademark of AAAS.